Delft University of Technology
Department of Chemical Technology
Materials for Energy Conversion and Storage

Global Climate and Energy Project

Advanced Membrane Reactors in Energy Systems; A carbon-free conversion of fossil fuels

Reporting period: May 2007 - April 2008

T.H.Y Tran
K. Stoitsas
W. Haije
J. Schoonman

Delft-The Netherlands, May 2008

Investigators

Joop Schoonman, Professor of Inorganic Chemistry; Wim Haije, Senior Scientist ECN, Kostas Stoitsas, post-doctoral researcher, Thi Hoang Yen Tran, PhD student.

Abstract

The deposition of aluminium oxide on the pore walls of mesoporous membranes, using trimethylaluminium and water vapour as precursors in the Atomic Layer Deposition (ALD) process is the subject of the first part of this report. The characterization of the membranes before and after modification with ALD was performed by using gas permeation and separation in a single or a mixed gas: H_2/CO_2. The gas permeance results are used to interpret the influence of the preparative ALD process on the pore size or number reduction and the hydrogen to carbon dioxide selectivity. Preliminary RF magnetron sputtering results are performed and presented in this report. Sputtering deposition will be studied in order to see the effect on pore size reduction. The modification of the surface characteristics and as a consequence the hydrothermal stability of membranes has been examined after deposition with sputtering.

In the second part of the report positron annihilation lifetime spectroscopy (PALS) measurements on the present micro and meso porous materials are presented. The purpose of this study is the structural characterization of porous materials using the gas adsorption technique and the positron beam analysis (PBA). PBA is one of the few techniques capable of probing the pore size and distribution in the nanometer scale [1].

Introduction

Much more efficient gas separation can, in general, be achieved if the pore diameters are reduced to molecular dimensions (smaller than 1nm), i.e., below the Knudsen regime. Although the Atomic Layer Deposition (ALD) process is extensively studied since the past decade, few efforts have been focused on the possibility of reducing the pore diameter of porous inorganic membranes to molecular dimensions [2-4].

The present study is focused on the development of the ALD process to prepare membranes for hydrogen separation.

The main activities in the short and long term are:

1. Development of membranes with mesopores using the sol-gel technique. Results have been published in the previous GCEP reports.
2. Modification of the appropriate membranes using the ALD process. Characterization of the modified membranes to study the effect of a deposited alumina layer on the pore size reduction, as well as H_2/CO_2 permeation and H_2 selectivity.
3. New characterization techniques for the structure of our micro-and mesoporous materials.

Results

Characterisation of primary γ-Al_2O_3 membranes

In the previous Progress Report (August 2006 - April 2007) the chemistry and the synthesis of thin films of γ-Al_2O_3 membranes was described. Also permporometry results confirmed the crack free character of these membranes. The pore size of these membranes according to the permporometry curve is around 3 nm.

In this study supported γ-Al_2O_3 membranes provided by Twente University were also used as substrates for ALD modification. This alumina membrane is disk-shaped (diameter: 39 mm, thickness: 2mm) with an asymmetric structure consisting of several layers with the final top layer having pores with radius 2-3 nm, and a porosity of 30%. More details of the preparation of this mesoporous membrane have been published by Chowdhury et al. [5]

Modification with Atomic Layer Deposition

The membranes were heated at 673K at atmospheric pressure to remove any organic and especially water vapour contamination at the surface before introducing them into the reactor chamber of the ALD equipment. The degassed membranes were flushed with nitrogen overnight to remove any adsorbed gas species during the transfer. The schematic of the ALD apparatus is shown in **Figure 1**.

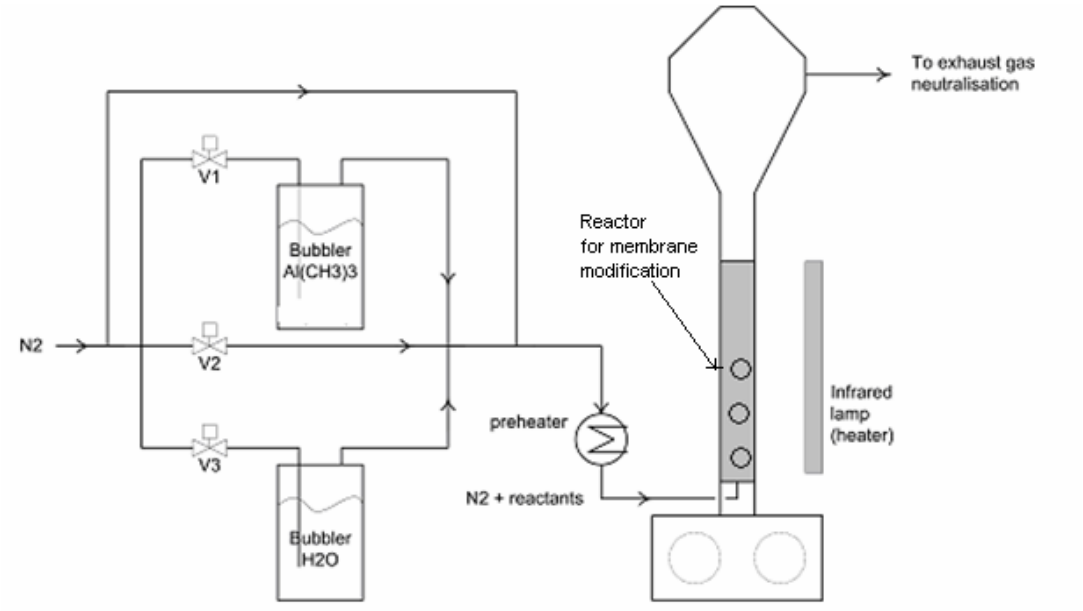

Figure 1: The schematic diagram of the ALD set-up.

The reactor chamber consists of a 26 mm internal diameter, 500 mm long glass reactor tube, in which the membranes were placed. The reactor was placed between 2 infrared lamps. The temperature inside the reactor is controlled by a thermocouple connected to the membrane holder. The sample holder comprises a steel base in which three supported membranes are mounted and each is clamped by two bars of two mm. The steel base is $20 \cdot 400 \cdot 3$ mm^3, and has a mass of 0.37 kg such that it can be assumed that has a homogenous temperature of 433 K. The membranes are mounted in such a way that the top layer is in contact with the ALD precursor gas atmosphere.

Each ALD-cycle consists of four process steps. These are: Valve V1 is opened, so that part of the nitrogen is led through a bubbler containing the trimethylaluminium ($Al(CH_3)_3$, TMA, Aldrich purity) precursor and saturated with its vapour. This vapour adsorbs to the surface of the membrane.

1. When the complete porous structure of the membrane is covered with the precursor, the valve V1 is closed and valve V2 is opened to purge the reactor tube with pure nitrogen. This removes the non-adsorbed TMA and CH_4.
2. Valve V2 is closed and valve V3 opened to lead the nitrogen gas through a bubbler containing water (temperature: relative humidity). The water vapour reacts with the $Al(CH_3)_3$ on the surface of the membrane.
3. Valve V2 is opened again and valve V3 closed to purge the reactor tube in order to remove the gaseous product.

In the present experiments, the deposition is carried out applying four cycles, with exposure time of the precursors and flushing nitrogen of 1:1:1:1 (10min of TMA-10min nitrogen-10min H_2O-10min nitrogen) at 433K. The flux through the bubblers is 100 cm^3 min^{-1} at 294K. The pressure of the reactor remains constant at 100 kPa. Our ALD reactor can not be used with TMA because the use of TMA requires extreme security measures.

Membrane characterization with gas permeation

Gas permeation experiments were performed at 303- 443 K using H_2, CO_2, H_2/CO_2 (50:50 v/v). A simple schematic diagram of the gas permeation equipment is shown in **Figure 2**.

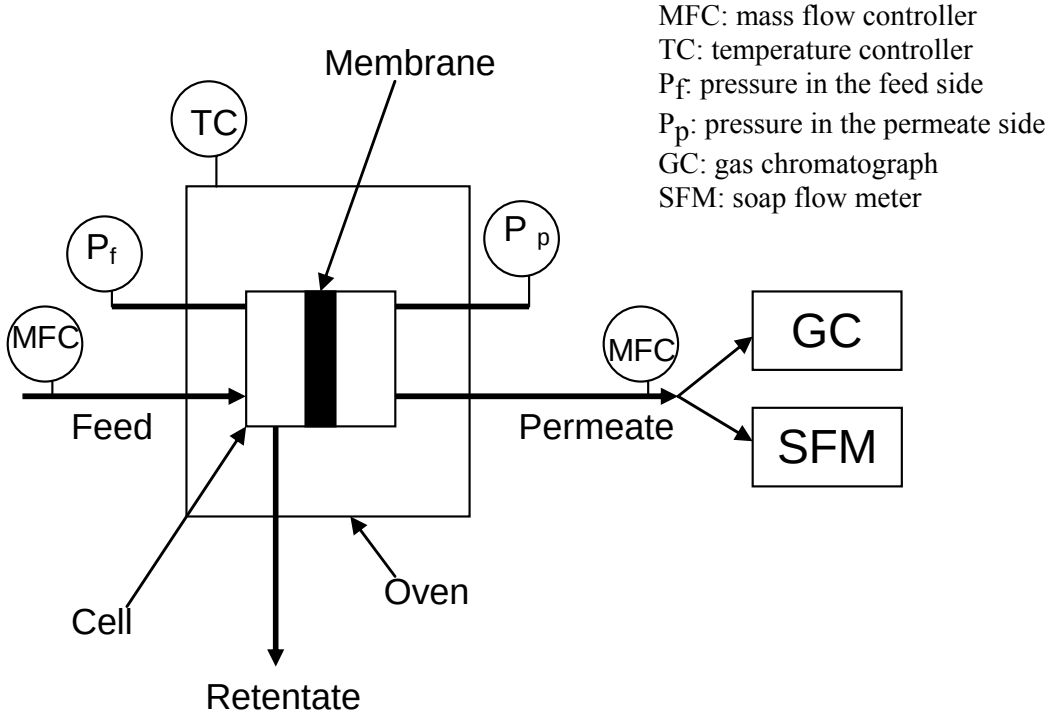

Figure 2: The schematic diagram of the permeation equipment.

The permeation flow rate was measured by a soap bubble flow meter. The permeance F (mol $m^{-2}s^{-1}Pa^{-1}$) of the gas permeating through the membrane is defined as:

$$F = \frac{J}{\Delta PA} \tag{1}$$

Where F is the gas permeance of the membrane (mol $m^{-2}s^{-1}Pa^{-1}$), J is the gas flow through the membrane (mol s^{-1}), ΔP is the pressure drop across the membrane (Pa), and A is the exposed area of the membrane (m^2).

The system consists of a membrane cell, pressure controllers, furnace, temperature controller, and mass flow meter. The permeate side of the membrane is kept at atmospheric pressure and the pressure of the feed side is controlled in the range of 100-500 kPa using a back pressure controller. The flow rates of gases are controlled by six mass-flow controllers. Before the experiments the membrane cell was fluxed with Helium at 373K overnight to remove adsorbed water from the nano-porous structure. The gas compositions were analyzed by gas chromatography (Varian Micro-GC4900) with a FID detector and CP-Sil-5 column.

Preliminary permeance results with modified γ-Al_2O_3 membranes are shown in **Figure 3**. The He premeance is almost 2 orders of magnitude smaller than the unmodified one, indicating that infiltration of aluminium oxide in the porous structure takes place.

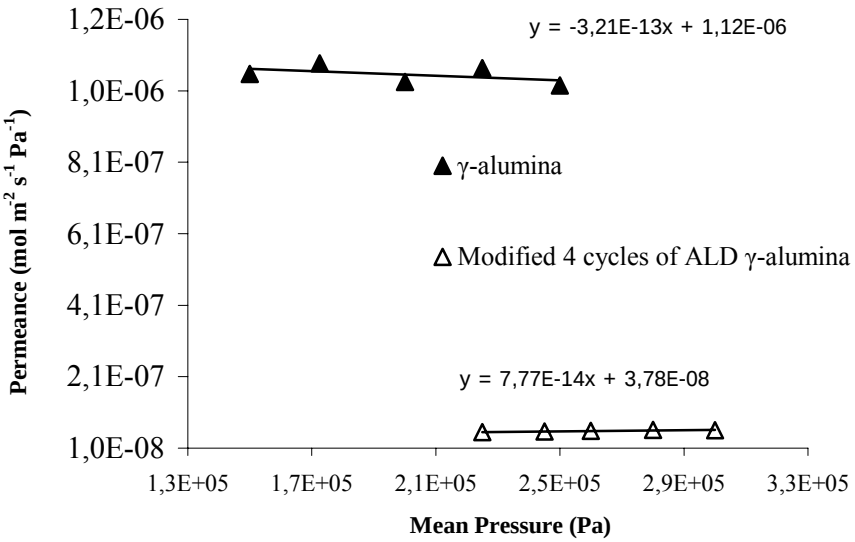

Figure 3: He permeance at 295K for unmodified and modified 4 ALD cycles γ-Al_2O_3 membranes.

Subsequently, the hydrogen and carbon dioxide permeances through this γ-alumina membrane before and after four cycles of ALD were studied as shown in **Figures 4 and 5**.

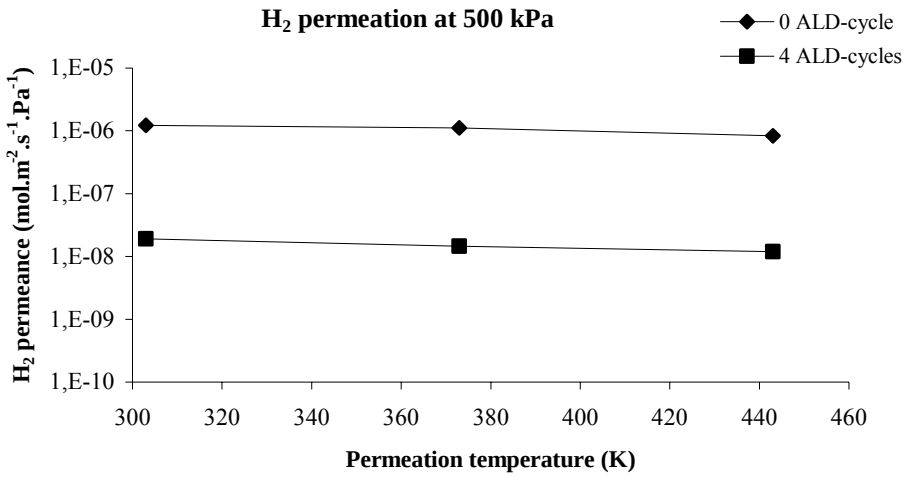

Figure 4: H_2 permeance for unmodified and ALD-modified γ-alumina membranes.

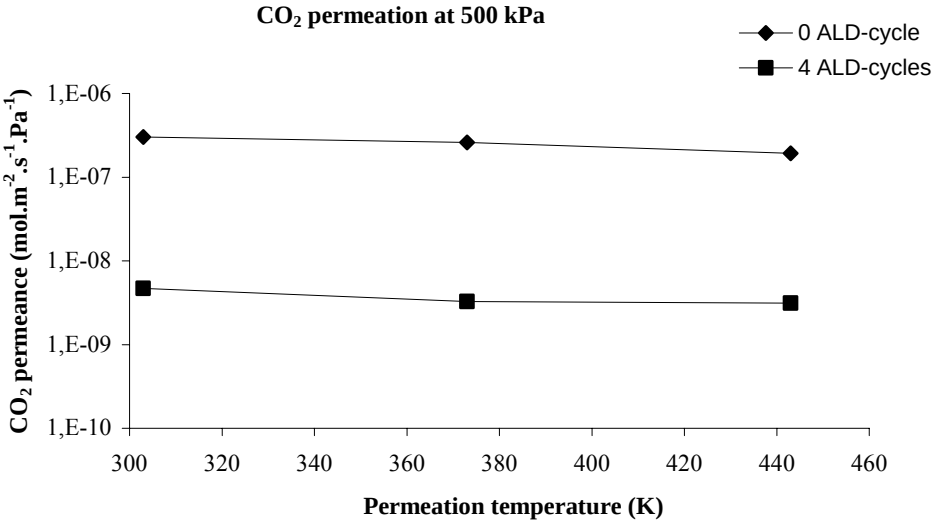

Figure 5: CO_2 permeance for unmodified and ALD-modified γ-alumina membranes.

The permeance values of H_2 and CO_2 decrease from $1.2 \cdot 10^{-6}$ and $3 \cdot 10^{-7}$ mol m^{-2} s^{-1} Pa^{-1} to $1.9 \cdot 10^{-8}$ and $4.7 \cdot 10^{-9}$ mol m^{-2} s^{-1} Pa^{-1} at 303K, respectively, after ALD. The modified γ-alumina membrane exhibits a permeance two orders of magnitude smaller than that of the unmodified membrane. The permeance of H_2 is higher than that of CO_2 because of its smaller molecular weight and weakest adsorption affinity relative to the surface sites of the membrane. The permeance slightly decreases with increasing permeation temperature, indicating the gas permeation follows the dominant Knudsen diffusion mechanism and the membrane remains mesoporous.

Figure 6 shows the effect of the temperature on the H_2/CO_2 separation factor for the γ-alumina membrane. The separation factor slightly increases with increasing permeation temperatures. When the temperature increases, the average molecular velocity increases and the adsorption of CO_2 at the surface of the membrane becomes weaker. The separation factor is lower than the permselectivity due to the interactions

between the gas molecules, even if the dominant transport mechanism is Knudsen diffusion in the membrane.

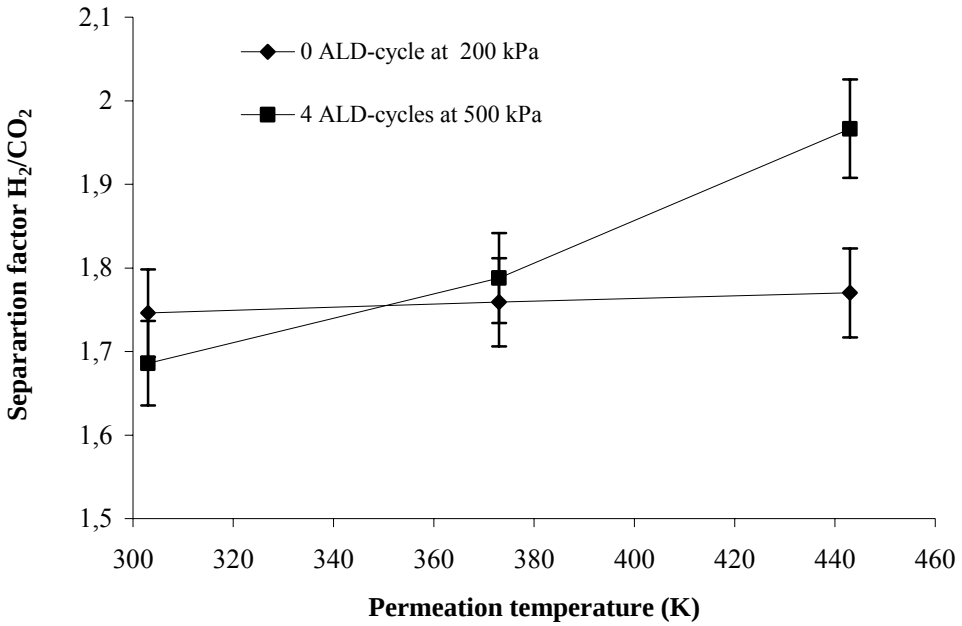

Figure 6: Separation factor for H_2/CO_2 for unmodified and ALD-modified γ-alumina membranes.

Membrane modification with sputtering technique

Preliminary experiments on the modification of sol-gel derived mesoporous silica membranes (MSM) were carried out by sputtering with Al_2O_3 or yttria-stabilized zirconia (YSZ).

The monodisperse mesoporous silica membrane was prepared from a silica sol, which was synthesized by dropping aqueous HNO_3 (1N) in a solution of tetraethylorthosilicate (TEOS, 98% purity, Aldrich) and 1-propanol (99.9% purity, Chromasolv) [5]. After five minutes the templating agent cetyltrimethylammonium bromide (CTAB, 99% purity, Aldrich) was added. The molar ratio of the final mixture was TEOS/CTAB/1-propanol/H_2O/HNO_3 = 1:0.13:15:15.5:0.14. The sol was heated at boiling temperature for two hours under reflux conditions. The α-Al_2O_3 support (NGK©) was dip coated in the sol mixture, which consisted of 15 ml of silica sol mixed with a modified urea solution referred to as BYK-420 (BYK-Chemie, Wesel, Germany). Drying at 313K for three hours and a calcination step in air at 873K for three hours with controlled heating and cooling rates followed after the dip-coating step.

The physisorption isotherm and the corresponding pore size distribution for the MSM films are presented in **Figure 7.** MSM films are chacterized by mesopores of 2-4 nm. Hysteresis is not present between adsorption-desorption because pores are straight and cylindrical so network effects for these materials are negligible.

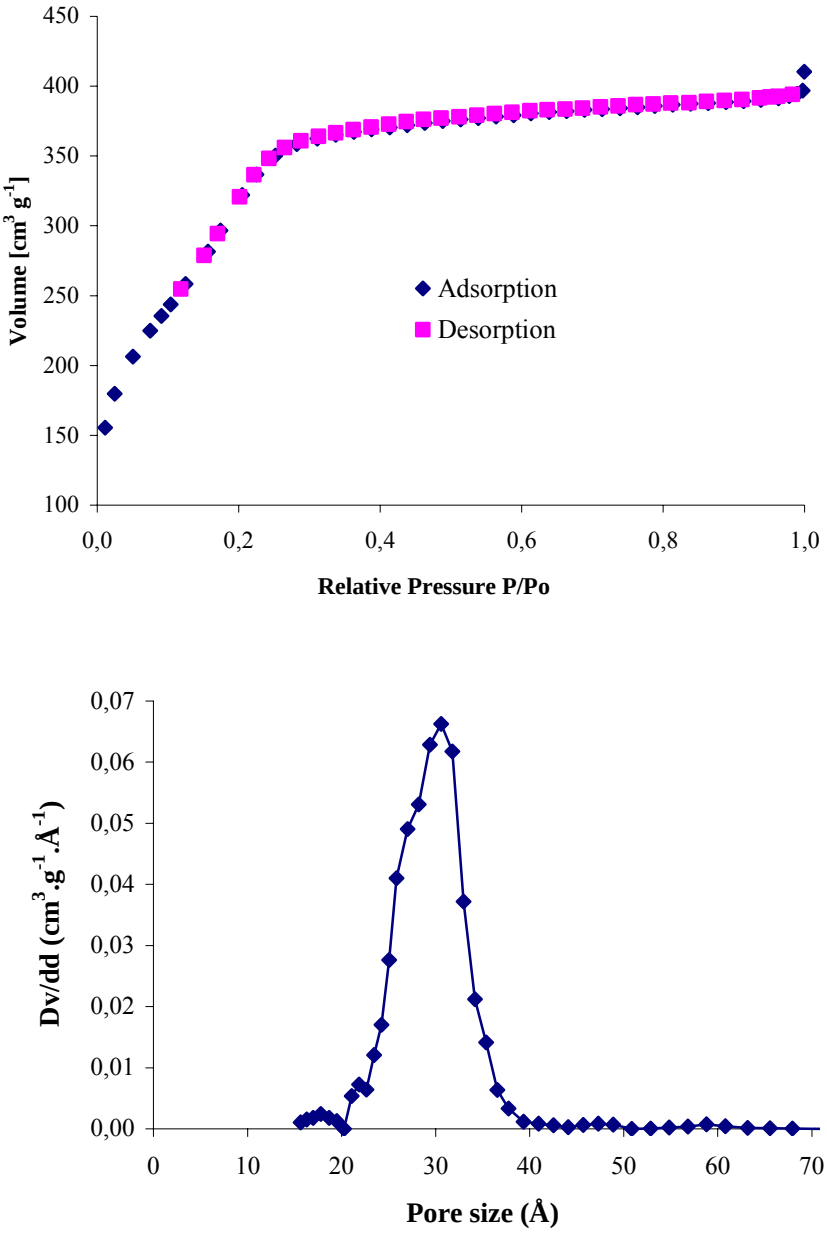

Figure 7: Physisorption isotherm (up) and pore size distribution (down) for MSM.

This coating is expected to modify the pores so as to shrink the pore entrance to the kinetic diameter of H_2. The coating with alumina or zirconia, which is more stable than silica under hydrothermal conditions, can protect the material under process conditions. The deposition was performed by a sputtering method, using an RF magnetron producing Ar plasma and using an α-Al_2O_3 or YSZ target to produce an Al_2O_3 or YSZ layer respectively. The deposition process was carried out in an RF sputtering equipment (ATC ORIOM 5HV, AJA International, USA), illustrated in **Figure 8**.

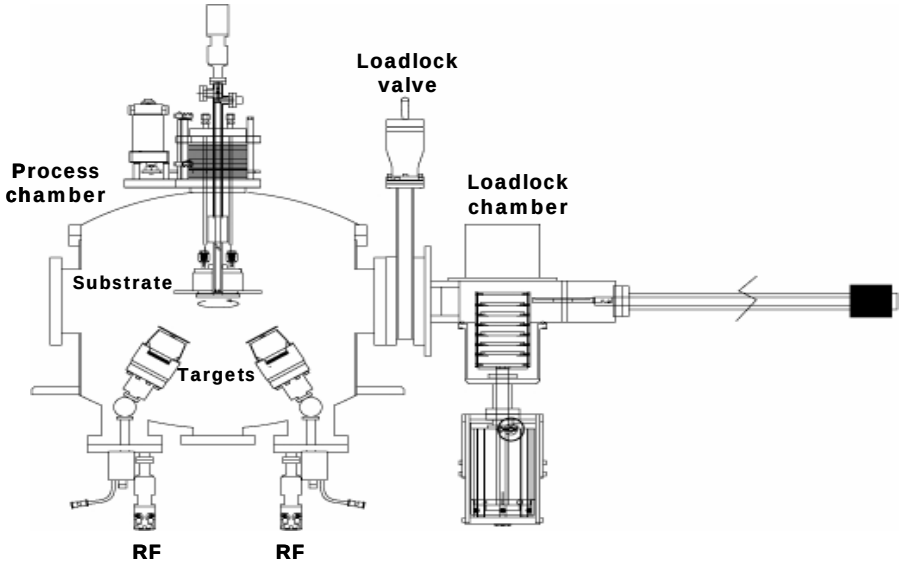

Figure 8: Schematic diagram of the sputtering equipment

The deposition parameters are summarised in **Table 1**.

Table I: Operating conditions for RF magnetron sputtering of alumina and YSZ.

Parameters	Al_2O_3 deposition	YSZ deposition
Working pressure	0.6 Pa	1.1 Pa
Flow rate of argon	8 cm^3 min^{-1}	14 cm^3 min^{-1}
Substrate temperature	673K	673K
Substrate–target distance	100mm	100mm
Power source	150 W	100 W
Time deposition	60min	60min
Target	Al_2O_3	YSZ
Substrate	Quartz, MSM film	Quartz, MSM film
Mean rate of film deposition	~ 1nm min^{-1}	~ 4nm min^{-1}

The structural analysis of the deposited films on the quartz substrates was to be carried out with an X-ray diffractometer (type Bruker D8 Advance). The diffraction patterns, shown in **Figures 9** reveal alumina film deposited by sputtering to be amorphous and the one of YSZ to be crystalline. The thicknesses of these films are estimated about 60nm for alumina and 250 nm for YSZ, based on the deposited growth rate.

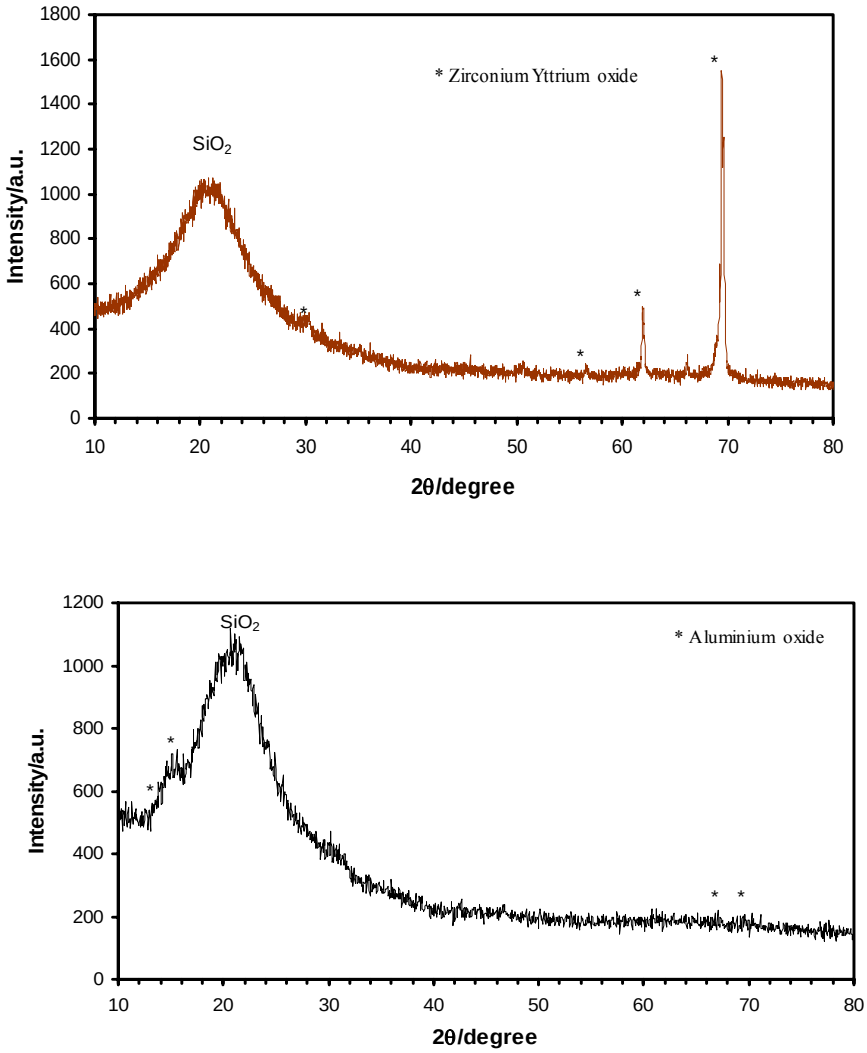

Figure 9: XRD diffraction patterns of zirconia (up) and alumina (down) sputtered on quartz.

For the first coating of MSM with the thichness of ~100nm, the He permeance value is similar to that of γ-alumina support as shown in **Figure 10 (a)**. This permeance decreases with the second coating MSM silica layer with the thichness ~ 200nm, as shown in **Figure 11 (a)**. This second layer allows covering the defects on the membranes.

Figures 10 (b) and 11 (b) show that the permeance values of He slightly decrease after alumina or YSZ sputter deposition. The results indicate that alumina and YSZ are deposited on the porous surface of the membranes. Since the He permeance is independent of the mean transmembrane pressure this still indicates predominant Knudsen behaviour the selectivity remains low. Further characterisations of the changes in pore structure of the membranes as a function of sputter deposition conditions will be performed, such as the permporometry, real gas separation experiments, Transmission Electron Microscopy (TEM), and the Atomic Force Microscopy (AFM) in order to establish in detail the results. The improvement of the stability of these membranes will also be studied in the next period.

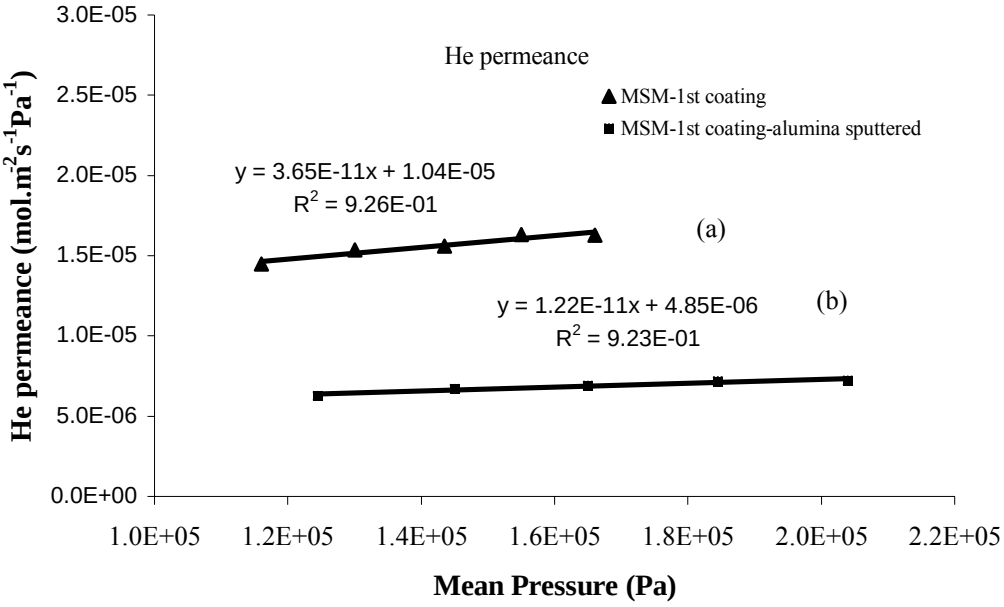

Figure 10: He permeance of (a) MSM prepared with one coating on γ-alumina and (b) Alumina sputtered on MSM prepared with one coating on γ-alumina.

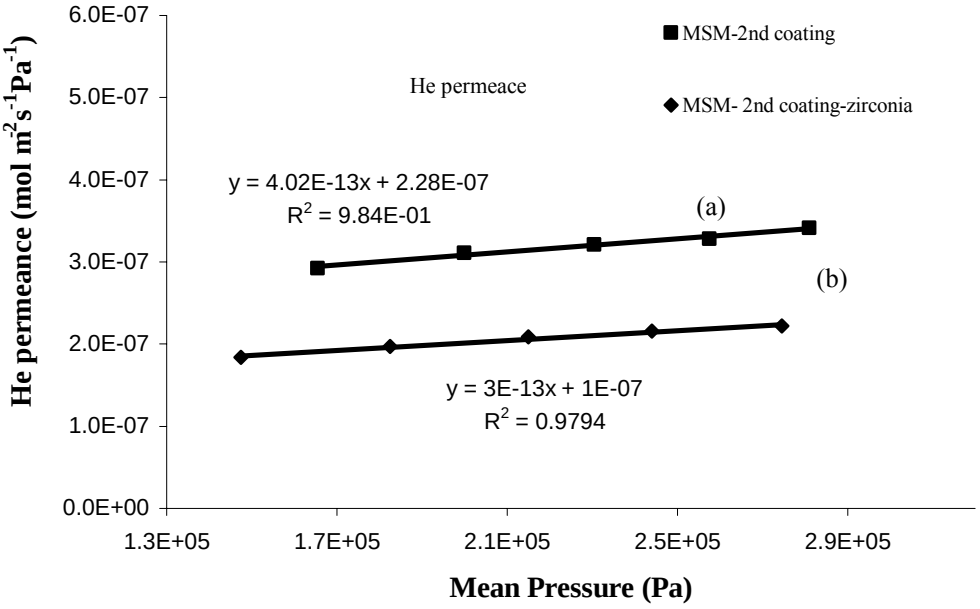

Figure 11: He permeance of (a) MSM prepared with two coatings on γ-alumina and (b) YSZ sputtered on MSM prepared with two coatings on γ-alumina.

Pore size evolution in alumina-silica hybrid materials for membrane applications: Characterization with N_2 physisorption and positron annihilation

In the previous reports the synthesis of self-supported alumina, silica, and binary samples was described. The samples have mesoporous, microporous or a combination of both structures. The porous networks developed were characterised in terms of pore size and surface area by means of N_2 sorption-desorption isotherms at 77K

(AUTOSORB 1-MP, Quantachrome Instruments). The samples before the measurements are out-gassed overnight at 423K under vacuum (10^{-1} Pa). For the determination of the pore size distribution the Density Functional Theory and the Horvath Kawazoe model were used for the mesopores and micropores, membranes, respectively [7,8].

In this study the Positron Beam Analysis (PBA) experiments were performed at the Delft Variable Positron beam facility. Positrons emitted from a ^{22}Na source are after moderation to thermal energies and subsequent acceleration injected into the samples with energies tuned between 0,1 keV and 25 keV. The beam intensity is about 10^4 positrons per second with beam diameter at target of 8 mm. The positron mean implantation depth <z> scales with the implantation energy according to,

$$<z> = A/ \rho \cdot E^{1,62} \qquad (2)$$

with A = 4 μg cm^{-1} keV$^{-1,62}$ a material independent parameter, ρ the density (g cm^{-3}), and E the positron implantation energy (keV). In materials with ρ ~ 4 g cm^{-3} the maximum implantation energy corresponds to an implantation depth of about 2 μm.

A thermalised positron ultimately annihilates with an electron resulting in most cases in the emission of two 511 keV gamma quanta. The momentum of the electron in the direction of the gamma emission ($p_{//}$) introduces a Doppler shift in the energy of the gamma given by $\Delta E = ½ cp_{//}$. In an annihilation gamma spectrum these shifts lead to a broadening of the 511 keV photo peak, which is quantified by the so-called S and W parameters. The S(hape) parameter is calculated as the ratio of number of events counted in a fixed momentum window ($|p_{//}| < 3,5 \cdot 10^{-3}$ $m_o c$) around the center of the peak to the total number of counts and is sensitive to annihilations with low momentum valence electrons. Similarly, the W(ing) parameter is obtained from the interval $10 \cdot 10^{-3}$ $m_o c < |p_{//}| < 30 \times 10^{-3}$ $m_o c$ and accounts for annihilations with high momentum core electrons. In general, at an open volume defect (such as vacancies or vacancy clusters) the probability of annihilations with core electrons is reduced resulting in a higher S parameter and lower W parameter value.

In large open volumes positrons may bind to an electron to form positronium, (Ps). In case the spins of the electron and positron are anti-parallel, para-Ps (p-Ps) is formed which decays into two 511 keV gammas with a lifetime $\tau_{p\text{-}Ps}$ of 125 ps. Ortho-Ps consists of an electron-positron state with parallel electron and positron spins. In vacuum the lifetime of this component $\tau_{o\text{-}Ps}$ is 142 ns and it decays into 3 gammas with energies distributed from zero to 511 keV. In solids the o-Ps lifetime is reduced to several nanoseconds due to spin-exchange or pick-off reactions with the electrons form the surface of the open volume. Both reactions result in the emission of two 511 keV gammas. For even larger cavities (including the surface) the o-Ps conversion reaction rates become slow in comparison to the o-Ps intrinsic decay rate ($=1/\tau_{o\text{-}Ps}$) and thus annihilation via 3 gamma emission becomes feasible. In the annihilation spectrum o-Ps decay is observed as an increase of counts below 511 keV. The relative amount of o-Ps decay is quantified by $(R\text{-}R_o)/R_o$ where R is defined as (T-P)/P with T the number of counts in the energy range from 100 to 511 keV and P the number of counts accumulated in a region centered around 511 keV. R_o is the value obtained when no Ps is formed.

Nitrogen adsorption-desorption isotherms of γ-Al_2O_3, SiO_2, and a binary sample are presented in **Figure 12**.

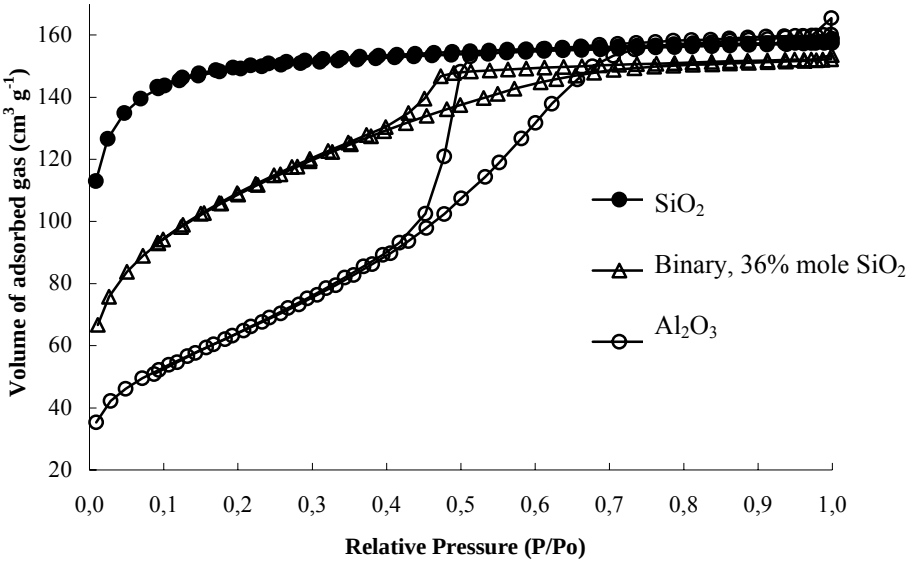

Figure 12: Nitrogen adsorption-desorption isotherms for γ-alumina, silica and binary layers.

Nitrogen physisorption isotherms of γ-Al_2O_3 and binary membranes are of type IV, typical for mesoporous solids [8]. The BET surface area of γ-Al_2O_3 is estimated at 280 m^2 g^{-1} using BET equation at low relative pressures while the porosity is estimated to be 48%. For the binary material the total pore volume is slightly reduced in comparison with pure γ-Al_2O_3 films. The binary sample is mainly mesoporous but micropores are also present in the structure. As can be seen the volume of the adsorbed gas is almost doubled at low relative pressures characteristic of the presence of micropores in the structure. The BET surface area of the binary membranes is 380 m^2 g^{-1}, higher than the pure γ-Al_2O_3 membranes due to the presence of microporosity in the structure.

On the other hand the corresponding results for pure SiO_2 show a type I isotherm which is characteristic for totally microporous solids [9]. The surface area of the SiO_2 membranes is 480 m^2 g^{-1}, while the total pore volume is similar to the pore volume of pure γ-Al_2O_3. The pore volume is similar for all the samples. SiO_2 membrane is expected to have higher pore volume. However, sintering effects, at final firing temperature of 873K, are dominant in the case of SiO_2 membranes resulting in more dense structures [10]. In **Table 2** the structural characteristics of the 3 samples are presented.

Table II: Structural characteristics for γ-alumina, silica and binary membrane layers

Samples	**Al_2O_3**	**Binary 36% mole SiO_2**	**SiO_2**
BET Area (m^2 g^{-1})	280	380	480
Pore Volume (ml (liq. N_2) g^{-1})	0,23	~0,23	0,23
Mean Pore Diameter (nm)	5,5	Bimodal (0,55 and 3)	< 2

The pore volume is calculated from the adsorbed gas volume ($cm^3\ g^{-1}$) at 1 atm and 273K assuming ideal gas and by choosing a correct estimate for the density of the adsorbed phase. According to the Gurvitsch rule, the calculated pore volume is then independent of the adsorptive provided that the pore volume is accessible for these gases [11]. For N_2 as adsorptive gas:

$$V_p\ (ml(liq.\ N_2)/g) = V_{ads}\ (ml(STP)/g) \cdot (1{,}547 \cdot 10^{-3}) \qquad (3)$$

Where the density of the N_2 in the pores was assumed to be 0,808 g ml^{-1}, which is the density of liquid N_2 at 77K.

In **Figure 13** the pore size distributions of the 3 samples are presented using the Density Functional Theory.

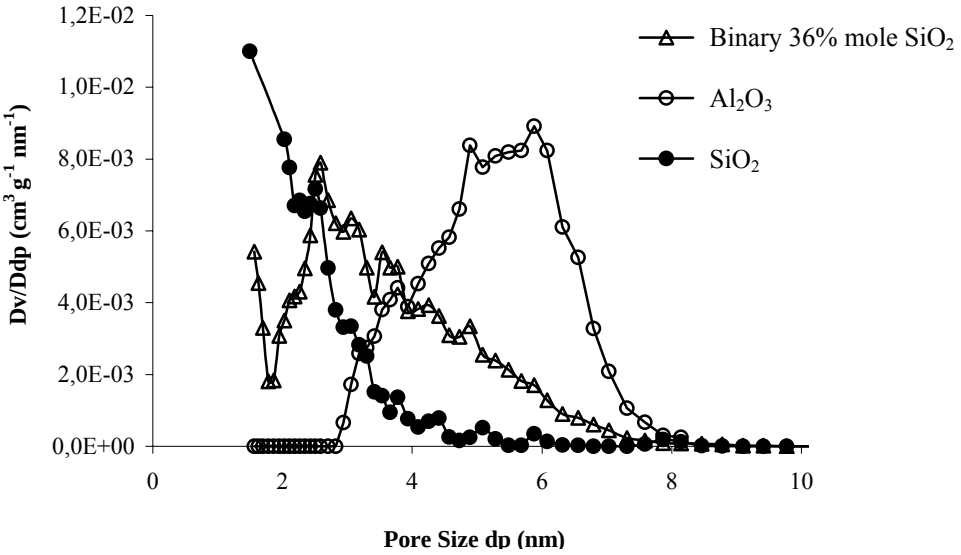

Figure 13: Pore size distribution of pure Al_2O_3, binary sample 36 mole % SiO_2, and pure SiO_2 using Density Functional Theory.

Pure γ-Al_2O_3 is characterized by a wide pore size distribution with a pore size of 3 to 8 nm. In the case of the binary sample the pores have a size of 2 to 7 nm. The difference between these samples is that the peak of the distribution for the binary sample is around 3 nm. On the other hand the pure sample has a smoother pore size distribution and the peak is moved to higher values of 5-6 nm. In addition, the binary sample is characterized by a bimodal pore size distribution, as it can be seen from the results obtained using the Horvath-Kawazoe model in **Figure 14** and the results obtained from the DFT model in **Figure 13**.

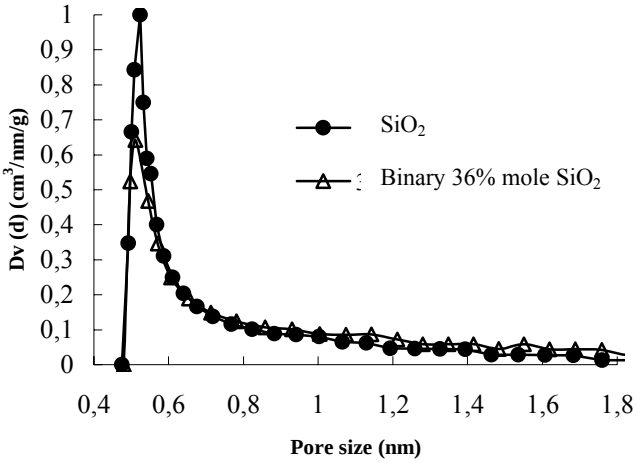

Figure 14: Pore size distribution of pure silica and the binary sample 36 mol % SiO_2 using the Horvath Kawazoe model for the micropores.

Pure SiO_2 is a completely microporous sample with a mean pore size of 0,55 nm. However, there are pores with sizes up to 1,8 nm. The mesoporous binary sample contains also micropores with the same size (0,55 nm) but the volume of the micropores for this sample is much smaller than the pore volume of the pure SiO_2. This is in agreement with the fact that the total pore volume is the same for both samples.

From the R parameter data a clear distinction can be made between the pure γ-Al_2O_3 and SiO_2 and the binary sample.

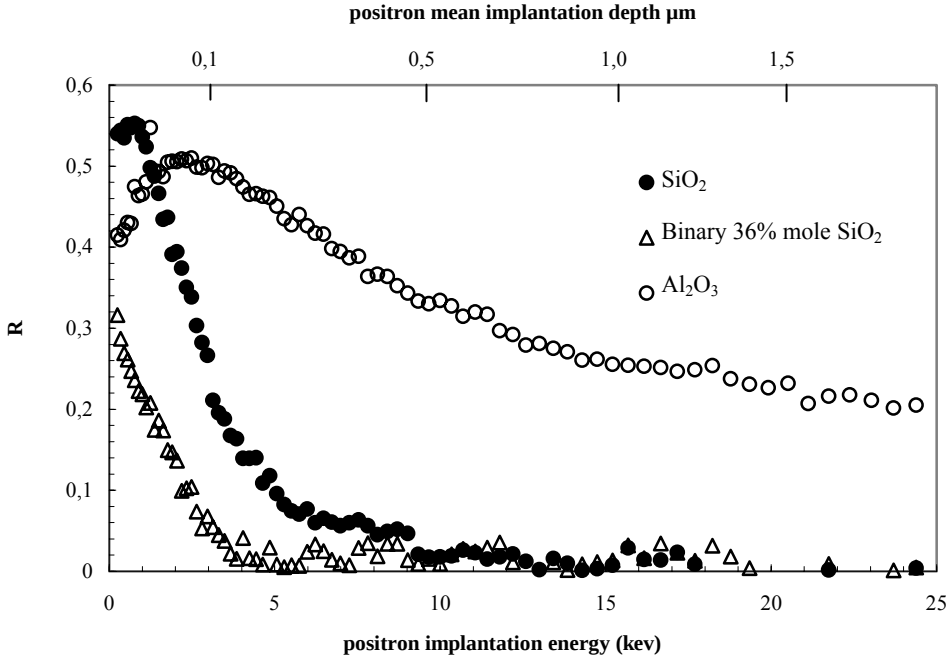

Figure 15: The R parameter as a function of positron implantation energy (bottom axis) and corresponding mean implantation depth (top axis).

The binary sample only shows a relevant amount of 3 gamma decay events up to a depth of approximately 70 nm. This is attributed to low energy positrons which during

the slowing down have back-scattered to the surface of incidence without becoming fully thermalised. When passing the surface they can pick-up an electron and are emitted as non-thermal or fast Ps (o-Ps and p-Ps). For the pure silica sample the o-Ps signal extends to somewhat larger depths. This is attributed to back-diffusion of thermalised positrons to the surface followed by the emission of thermal Ps. In the S parameter data for the mixed sample a minimum is observed at an energy of about 3,5 keV corresponding with the onset of 3 gamma decay detection. The minimum indicates the presence of a sub-surface region or interface effectively trapping positrons and thus preventing back diffusion of thermal positrons towards the surface. This asymmetry structure created in the binary material is possibly related with the asymmetry in the drying of the film. The one face is open to the ambient enabling quick drying by evaporation. On the other hand the side in contact with the petry dish lacks this quick evaporation pathway. The general trend in the R data for the silica and binary sample shows that no 3 gamma decay occurs in the bulk of the material, in contrast to pure γ-Al_2O_3.

In the S parameter data in **Figure 16** no such significant difference between pure γ-Al_2O_3 and SiO_2 is seen.

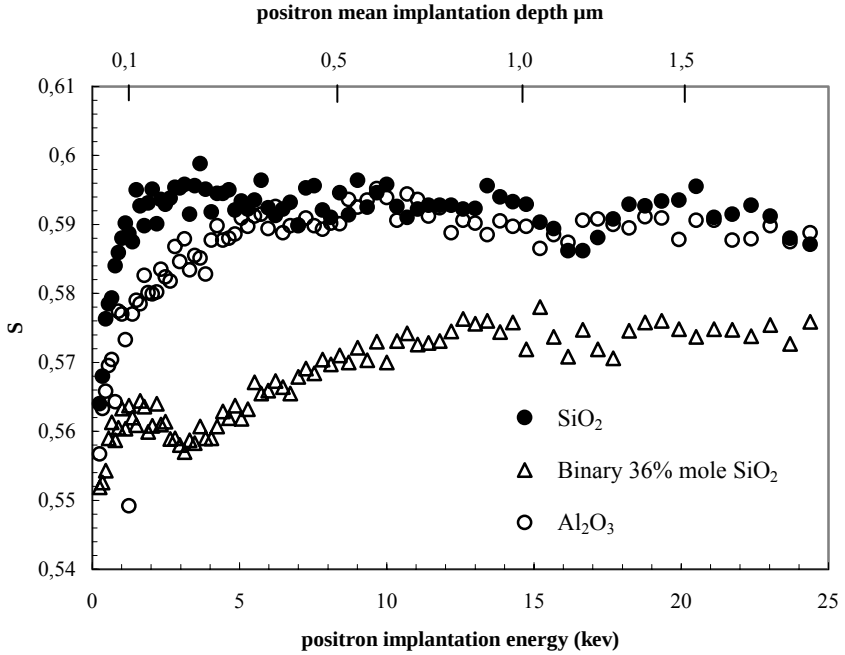

Figure 16: The S parameter as a function of positron implantation energy (bottom axis) and corresponding mean implantation depth (top axis).

In this case the composite sample shows a general lower S in the bulk. The origin of the difference in the near surface region is explained above. The apparent difference in R and S dependence can be accounted for by constructing a branching scheme for the different positron annihilation channels. This has been shown by Escobar et al. for positron studies of internal pore surfaces in low *k* silica films [12]. However, on the basis of the limited data in the present study only a qualitative description can be given.

The general picture emerging from the positron data is that in the pure γ-Al_2O_3 cavities are present which are large enough to accommodate Ps formation and the

subsequent decay from the o-Ps state. The silica sample shows no sign of o-Ps decay, putting an upper limit to the cavity size. The high value of S (within the experimental uncertainty equal to that of alumina) is attributed to the intrinsic decay of p-Ps. With the settings of the momentum windows for determining the S parameter p-Ps decay is expected to yield an S of approximately 0,75. The fraction of positrons annihilating from this state accounts for the observed value of S and thus hints at the formation of Ps.

In the composite sample no o-Ps is observed. In addition, the low S value indicates that no p-Ps decay is involved. This interpretation leads to the conclusion that positrons in the composite sample mainly annihilate at sites with dimensions too small for Ps formation.

This qualitative picture is in accordance with the observations obtained by the N_2 adsorption-desorption measurements. For the pure γ-Al_2O_3 a mean pore diameter of 5,5 nm is obtained. From positron lifetime experiments in zeolites it is known that this is large enough to observe the intrinsic decay of o-Ps [13]. The pure SiO_2 has cavities with dimension smaller than 2 nm. These are large enough to open the channel for Ps formation, but evidently too small to allow for o-Ps decay. The binary sample shows a bimodal distribution with mean pore diameters of 0,55 and 3 nm. The former are apparently too small to enable Ps-formation. Moreover, they are present in a concentration to effectively trap positrons, thereby competing with formation of Ps in the larger (3 nm) cavities. The overall effect is thus seen as a lower S due to the reduced fraction of positrons decaying from p-Ps.

Conclusions

- Separation factor for H_2 still remains in the Knudsen regime after modification of γ-Al_2O_3 membranes with four cycles of ALD.
- Membranes with non-tortuous structures and narrow pore size distribution are necessary for ALD modification in order to obtain high selectivity for H_2.
- Positron annihilation confirms the pore sizes and pore size distributions found by N_2 physisorption in a qualitative way.
- Positron annihilation is able to provide detailed information about the asymmetry and in-homogeneity of porous materials (related possibly with the drying process).
- The composite material shows characteristics of both pure members e.g. micro and meso porosity, the homogeneity of this mixed phase, however, is only evidenced for the first few microns.

Future Plans

- A study about the hydrothermal stability of the membranes is in progress.
- Modification experiments with Atomic Layer Deposition and Sputtering for the development of microstructures with tailored pore size that will yield high separation factors for H_2 are in progress.

Publications

1. T.H.Y. Tran, K. Stoitsas, W. Haije, J. Scoonman, Pore size control of ceramic membranes by atomic layer deposition for hydrogen separation. International Conference on Inorganic Membranes (ICIMs) Tokyo, Japan (2008).
2. K. Stoitsas, T.H.Y. Tran, W. Haije, J. Schoonman. Synthesis, characterization and separation potential for H_2/CO_2 mixtures of Alumina and Silica membranes. (Oral Presentation) Lunteren (2008).
3. T.H.Y Tran, K. Stoitsas, W. Haije, J. Schoonman. Preparation and characterization of Alumina-Silica composite membranes for modification by Atomic Layer Deposition technique. (Poster Presentation) Lunteren (2007)
4. K. Stoitsas, T. Tran, W. Haije, J. Schoonman. Monodisperse Porous Support System for Atomic Layer Deposition for Pore Size Tuning of H_2-Selective Porous Membranes. (Poster Presentation) Lunteren (2007).

References

1. *P. Coleman, "Positron beams and their applications" World Scientific, Singapore, 2000.*
2. *A. W. Ott, J. W. Klaus, J. M. Johnson, S. M. George, K. C. McCarley, J. D. Wa, Chem. Mat. (1997) 707.*
3. *J. W. Elam, D. Routkevitch, P. P. Mardilovich, S. M. George. Chem. Mat. (2003) 3507.*
4. *S. Mahurin, L. Bao, W. Yan, C. Liang, S. Dai. J. Non-Cryst. Sol. (2006) 3280.*
5. *S. R. Chowdhury, R. Schmuhl, K. Keizer, J. E. ten Elshof, D. H. A. Blank. J. Membr. Sci. (2003) 177.*
6. *V. Boffa, J. E. ten Elshof, D. H. A. Blank. Micropor. and Mesopor. Mater. (2007) 173.*
7. *J. Rouquérol, D. Avnir, C.W. Fairbridge, D.H. Everett, J.H. Haynes, N. Pericone, J.D.F. Ramsay, K.S.W. Sing , K.K. Unger, Pure Appl. Chem. (1994) 1739.*
8. *G. Horvath, K. Kawazoe, J. Chem. Eng. Ja. (1983) 470.*
9. *B.J. Condon, "Surface area and porosity determinations by physisorption: measurements and theory" Amsterdam: Elsevier, 2006.*
10. *R. M. de Vos, H. Verweij, J. Membr. Sci. (1998) 37.*
11. *J. Schroder, GIT Fachz. Lab. (1986) 978.*
12. *R. Escobar, A. van Veen, H. Schut, S.W.H. Eijt, C.V. Falub, A.R. Balkenende and F.K. ten Theije, Mater. Engineer. B102 (2003) 403.*
13. *Zs. Kajcsos, L. Liskay, G. Duplâtre, K. Lázár,L. Lonilla, L. Varga, P.M. Gord, Ap. De Lima, C. Lopes de Gil, M.F. Ferreira Marques, D. Bosnar, S. Bosnar, C. Kosanovic, B. Subotic, Rad. Phys. Chem. (2007) 231.*

Acknowledgements

The authors are grateful to Dr Henk Schut for performing the Positron Beam Analysis. Prof. Freek Kapteijn and Dr. Ruud van Ommen are also acknowledged for providing us the equipment to do physisorption analysis and ALD experiments, respectively.